JOURNAL OF MATERIALS SCIENCE **36** (2001) 153–163

Synthesis of iron zircon coral by coprecipitation routes

M. LLUSAR*, J. CALBO, J. A. BADENES, M. A. TENA, G. MONRÓS
Inorganic Chemistry Area, Inorganic and Organic Chemistry Department, Jaume I University, Castellón, Spain
E-mail: mllusar@qio.uji.es

An iron-doped (15 mol-% of Fe_2O_3) zircon ceramic pigment has been prepared using binary (ZrO_2-Fe_2O_3 and SiO_2-Fe_2O_3) and ternary (ZrO_2-Fe_2O_3-SiO_2) colloidal gels or coprecipitates as precursors. The obtained raw powders, precalcines, and fired pigments have been characterized by XRD, thermal analysis (TGA/DTA) and SEM/EDX to analyze the effect of binary interactions (occlusion and adsorption phenomena) on the synthesis of the iron-zircon coral as well as on the coloring yield. The use of a binary raw coprecipitate as precursor prepared with colloidal silica and ferrous sulphate leads to a higher efficiency in the hematite occlusion, since a more intense coral hue ($L^* = 59.6$, $a^* = 29.3$ and $b^* = 25.8$ at 950°C) is obtained, similar to an optimal ceramic reference. The protection or occlusion of α-Fe_2O_3 in amorphous silica agglomerates of high specific surface appears to be a more effective reaction intermediate than the observed adsorption of micronic α-Fe_2O_3 particles on tetragonal zirconia monoliths. The necessary transformation of tetragonal zirconia into its monoclinic form prior to zircon formation, and the higher α-Fe_2O_3 segregation from the coprecipitate obtained with Zr and Fe precursors, seem to lower the efficiency of the hematite coarsening-occlusion process involved in the coral pigment formation.

1. Introduction

The iron zircon coral is one of the three zircon-based pigments (together with the vanadium zircon blue and the praseodimium zircon yellow), that are market leaders in high temperature applications owing to their intensity of color, brightness, and stability up to 1380°C in all types of glazes. The traditional ceramic synthesis of this pigment consists in mixing the appropriate Fe precursor ($FeSO_4 \cdot 7H_2O$ and FeO(OH) are recommendable) with zirconia, silica and different mineralizers (mainly alkaline halides), and subsequently firing to temperatures such as 900°C or higher. However, even though important attention has been devoted to this pigment within the last years, some controversy about the nature and mechanism of formation of this pigment still remains, which needs clarification.

Recent investigations of Berry *et al.* [1] on the ceramic synthesis of the pigment have found out that iron is present in the pigment not only as hematite (α-Fe_2O_3) inclusions but also as paramagnetic Fe^{3+} species forming solid solution in insterstitial rhombic and axial sites of the zircon lattice. The same authors conclude that at concentrations of iron (in the final pigment) higher than 1 mass %, the color properties are all dominated by the presence of the α-Fe_2O_3 inclusions, but it is not clear which of both contributions dominates the color properties at low iron concentrations, since both Fe^{3+} species in solid solution and hematite inclusions are found to coexist. More recently, Gair *et al.* [2] also confirm by XANES and EXAFS analyses the existence of two distinct coloring sources: 4-coordinated iron incorporated in the zircon lattice substituting for silicon (in disagreement with the interstitial location assumed by Berry *et al.*), which by itself only produce a cream color, and occluded discrete hematite particles, which are responsible for obtaining a good commercial coral red pigment. In this work, the amount of iron introduced into the zircon lattice is found to be higher by sol-gel routes than by the conventional ceramic method, but with these unconventional synthesis methods only a cream peach color is obtained instead of a red coral, due to the lower proportion of occluded hematite.

Therefore, the presence of hematite inclusions in the zircon matrix appears to be the main responsible for the commercial coral zircon color. With regard to this encapsulated nature of the pigment, Airey [3] proposes a reaction mechanism in which zircon grows around an iron oxide particle, trapping it. Lahuerta [4] also accepts the encapsulated nature of the pigment, and concludes that a satisfactory coloring performance of the pigment is not only due to an adequate development of the protecting microstructure, but also due to the hematite particles having the appropriate color. Llusar *et al.* [5, 6], in agreement with Airey, suggest a coarsening-occlusion

* Author to whom all correspondence should be addressed.

mechanism as a general model for the formation of the pigment. In this model, the processes of crystallization, synthering and occlusion are considered to take place simultaneously, and the kinetics of the reaction is considered to follow the nucleation-coarsening model observed by Eppler [7]. From optic and scanning electron microscopy observations, the authors also find the coloring performance to be closely related to the amount of colored zircon particles occluding hematite [6], and, therefore, the better the efficiency of hematite occlusion, the more intense the coral color. On the other hand, Eppler studies the mechanism of formation of zircon pigments in the presence of fluorides using the marker technique [8] and concludes that, while silica reacts with fluoride mineralizers to be vapor-transported to zirconia reaction sites (as SiF_4), iron remains in its place. Hence, it is considered that the iron oxide must be present at the reaction site prior to the zircon formation. However, the same author [9] doubts of the inclusion nature of the pigment, since a lot of the iron fails to react and remains as hematite impurity in the calcine.

Considering the role played by the mineralizers, their addition has been found effective to reduce the temperature of pigment formation. This can be achieved in different ways [5, 6] but basically two of these mineralizing processes seem to be determinant. Firstly, as previously commented, fluorides can facilitate the transport of silica to ZrO_2 reaction sites by the volatile SiF_4 species formed from the reaction between silica and NaF [8], in which the ferrous sulphate (iron precursor) also could be involved being oxidized to hematite and forming Na_2SO_4 [10]. And secondly, the formation of flux phases, such as the glassy phase formed between NaF and NaCl at temperatures compressed between 600 and 700°C (both form an euthectic around 674°C with a molar ratio NaCl : NaF equal to 2 : 1) can trigger the diffusion of reactants to form the pigment (Berry *et al.* [10] detect the formation of this glassy phase at 680°C with an equiponderal mixture of NaF and NaCl, which is very close to the temperature, around 700°C, at which zircon starts forming).

Nevertheless, even though these contributions of mineralizers to the kinetics of formation of the coral zircon pigment are very important, one must keep in mind that, finally, the "major" mechanism or process determining the final peach color is the effective occlusion of hematite by the nascent zircon particles. Assuming the relevance of obtaining an efficient inclusion of α-Fe_2O_3 particles, the existence of binary interactions between ZrO_2 and Fe_2O_3, and/or between SiO_2 and Fe_2O_3 also must be decisive in the synthesis, and should be analyzed with more attention to determine the most appropriate synthesis method and precursors to obtain an intense coral red pigment. In the study of Berry *et al.* [1], for instance, EPR studies of a calcined iron-impregnated zirconia seem to confirm the presence of Fe^{3+} species in low-symmetry sites on the ZrO_2 surface. In the same direction, Tartaj *et al.* also mention [11] the possible formation of a solid solution of Fe^{3+} in the tetragonal zirconia lattice as a reaction intermediate when preparing the iron zircon coral by pyrolysis of aerosols. As for the binary SiO_2-Fe_2O_3 interactions, the potential ability of amorphous SiO_2 as a host matrix to protect or occlude hematite particles cannot be neglected. In this respect, a stable red pigment can easily be prepared by occluding hematite (α-Fe_2O_3) in a silica matrix employing conventional or aqueous sol-gel processing routes [12, 13].

Accordingly, both Fe_2O_3-ZrO_2 and Fe_2O_3-SiO_2 binary interactions have proved to occur readily when firing intimate mixtures of these components obtained by unconventional synthesis methods. Thus, the employment of different precursors and/or synthesis methods seems to influence the reaction mechanism, since different intermediates can form, and, consequently, the efficiency accomplished in the hematite occlusion may not be the same. In this respect, sol-gel processing exhibits potential advantages to obtain highly reactive precursor systems [14], with a much more intimate mixture of the elements taking part in the solid-state reaction. In addition, the aqueous sol-gel processing has proved to be a good synthesis method to control the conditions needed for obtaining a good efficiency in the encapsulation of ceramic pigments of inlusion or heteromorphic nature [13].

In this paper, the synthesis of an iron zircon ceramic pigment by sol-gel or coprecipitation routes has been examined to see if any improvement can be made with respect to the ceramic method. Together with a reference composition prepared by the ceramic method and with a "complete" colloidal gel containing all the precursors and mineralizers, raw and precalcined intimate binary mixtures of Zr-Fe and Si-Fe also have been prepared by the coprecipitation route to be used as precursors in the synthesis of the pigment, and have been characterized by XRD and SEM/EDAX. The effect of binary interactions on the efficiency of hematite occlusion, and, therefore, on the coloring yield, has been analyzed.

2. Experimental

An optimized composition of the iron zircon coral [6], responding to the overall stoichiometry $(SiO_2)(ZrO_2)_{0.97}(Fe_2O_3)_{0.15}(NaF)_{0.7}(NaCl)_{0.3}$ was prepared by the traditional ceramic procedure and by aqueous sol-gel or coprecipitation procedures. Quartz and zirconia (baddeleyite) of commercial technical grade, supplied by Navarro (with $\phi_{50} = 3.9$ and 5.6 μm, respectively), and $FeSO_4 \cdot 7H_2O$ (Panreac) were used as Si, Zr and Fe precursors in the ceramic route; a fine colloidal silica (ϕ_{50} around 250 nm) of Quimidroga, and $ZrOCl_2 \cdot 8H_2O$ (Merck) were employed instead of the commercial oxides in the coprecipitation route. The iron precursor (ferrous sulphate) and the mineralizers (technical grade, commercial NaF and NaCl, also supplied by Navarro) were the same in both methods.

To prepare the reference ceramic composition (*CER sample*), the appropriate amounts of each precursor and mineralizers were mixed and ball-milled in acetone medium. Residual acetone was then removed by evaporation, and the resulting dried powder was finally homogenized in an agate mortar.

By using the aqueous sol-gel processing three different gels or coprecipitates were obtained. A complete colloidal gel (*CC sample*) was first prepared by adding the zirconium oxychloride to an aqueous suspension of the colloidal silica, with continuous stirring and heating at 70°C; two hours later, the ferrous sulphate was added and the resulting acidic mixture (pH = 2) was left under the same stirring and heating conditions for four hours before the addition of the mineralizers (NaF and NaCl); the viscosity of the mixture was observed to rise abruptly with mineralizer addition, and, therefore, a yellowish-brown gel was readily obtained at pH = 2-3 with the addition (dropwise) of a little amount of concentrated ammonia. A binary coprecipitate containing only the Si and Fe precursors (*SFC*) also was prepared by leaving the ferrous sulphate in an aqueous suspension of colloidal silica (continuously stirred and heated at 70°C) for 24 h. After this time, concentrated ammonia was added dropwise to the yellowish-orange acidic mixture (pH = 2), which did not produce a gel but a greenish-brown coprecipitate at pH = 4. Finally, a binary, yellow colloidal gel containing Zr and Fe precursors (*ZFC*) was obtained (at pH = 2) by adding dropwise concentrated ammonia to an aqueous solution of $ZrOCl_2 \cdot 8H_2O$ and $FeSO_4 \cdot 7H_2O$ kept at the same stirring and temperature (70°C) conditions.

The partial or complete raw gels (or coprecipitates) were dried under infrared (IR) lamps for 24 h and then homogenized in an agate mortar. The raw mixtures were not washed, since the presence of species that can act as heterogeneous nucleation agents (such as chlorides, and/or sulphates) can be used to improve the reactivity of the gels and/or coprecipitates [15–17], which is useful in the synthesis of heteromorphic pigments [13]. To accomplish the stoichiometry of the chosen iron zircon coral formulation, the appropriate amounts of the remaining silicon or zirconium precursors (commercial oxides) and mineralizers were added to the dried raw ZFC gel and to the SFC coprecipitate, and were ball-milled together in acetone medium. The resulting mixtures were dried under IR lamps and referenced as *ZFC1* and *SFC1* samples. In addition, to analyze the effect of using precalcines of binary ZrO_2-Fe_2O_3 and SiO_2-Fe_2O_3 mixtures as precursors, a portion of each of the dried raw ZFC and SFC coprecipitates were precalcined in Si-Al crucibles at 800°C for 2 h in an electric furnace. As before, the remaining Si or Zr precursors (oxides) and mineralizers were then added to these precalcined mixtures to obtain the desired iron zircon formulation. These samples were referenced as *ZFC2* and *SFC2*. The precursors, preparation methodology, and sample nomenclature employed is summarized in Table I.

Simultaneous Differential Thermal and Thermo-Gravimetric Analysis (DTA-TGA) was performed with a Mettler Toledo thermal analyzer on representative raw samples to aid in the understanding of the processes or reactions occurring during the firing of the samples. Thermal analysis was carried out in Pt crucibles with a constant 5°C/min heating from 25 up to 1100°C.

To obtain the iron zircon coral pigment, the dried powders were fired following a previously optimized firing schedule in an electric furnace up to 950°C, with heating and soaking times of 4 h and 2 h 30 min, respectively. Sample calcination took place in Si-Al crucibles filled completely with the raw powders, which were manually pressed and inverted upon a lid of the same Si-Al material. The resulting fired pigments were washed before being enameled following a standard procedure. Washing served to eliminate undesirable soluble salts that have negative effects during the enamel firing and to measure the Fe^{3+} and SO_4^{2-} concentration leached from the pigment in washing waters. With this purpose in mind, 1 g of each calcined composition was washed with 0.3 M HCl in the presence of Fe (acid-reductor washing) until 100 mL of washed waters were obtained. Washed-off Fe^{3+} was determined by colorimetric measurement at 475 nm with a Perkin-Elmer spectrophotometer of the complexes formed adding a tiocyanate solution in acidic media. On the other hand, SO_4^{2-} concentration in washing waters was gravimetrically determined by quantitative precipitation with 0.1 M $BaCl_2$.

In order to identify the crystalline phases present in the raw, precalcined (ZFC and SFC) and fired powders, X-ray Diffraction (XRD) patterns were obtained using conventional powder techniques in a Siemens D-5000 diffractometer with Ni-filtered, Cu K_α radiation and with a goniometer speed of 0.05 $^\circ 2\theta$/s (1s of counting time per step). A microstructural characterization and semiquantitative analysis of ZFC and SFC binary precalcines, and of representative (optimal) fired pigments were also carried out by scanning electron microscopy (SEM), using a Leo-440i Leyca microscope equipped with an energy dispersive X-ray analysis (EDAX) attachment supplied by Oxford University.

Washed pigments were finally enameled with a fritted transparent glaze adding a 5% of color in the glaze.

TABLE I Preparation methodology, precursors, and nomenclature of the samples

Sample	Precursors	Preparation Methodology
CER	ZrO_2 (baddeleyite), SiO_2 (quartz), $FeSO_4 \cdot 7H_2O$ (Panreac), NaF, NaCl	Ceramic procedure (ball-milling)
CC	$ZrOCl_2 \cdot 8H_2O$ (Merck), SiO_2 (colloidal, Quimidroga), $FeSO_4 \cdot 7H_2O$ (Panreac), NaF, NaCl	Colloidal gel with all the precursors and mineralizers
SFC1	SiO_2 (colloidal, Quimidroga), $FeSO_4 \cdot 7H2O$ (Panreac), ZrO_2 (baddeleyite), NaF, NaCl	Raw coprecipitate with Si and Fe precursors (SFC), ball-milled with ZrO_2 and mineralizers
SFC2	SiO_2 (colloidal, Quimidroga), $FeSO_4 \cdot 7H_2O$ (Panreac), ZrO_2 (baddeleyite), NaF, NaCl	Precalcined (800°C/2 h) SiO_2-Fe_2O_3 coprecipitate, ball-milled with ZrO_2 and mineralizers
ZFC1	$ZrOCl_2 \cdot 8H_2O$ (Merck), $FeSO_4 \cdot 7H_2O$ (Panreac), SiO_2 (quartz), NaF, NaCl	Raw gel with Zr and Fe precursors (ZFC), ball-milled with SiO_2 and mineralizers
ZFC2	$ZrOCl_2 \cdot 8H_2O$ (Merck), $FeSO_4 \cdot 7H_2O$ (Panreac), SiO_2 (quartz), NaF, NaCl	Precalcined (800°C/2 h) ZrO_2-Fe_2O_3 gel, ball-milled with SiO_2 and mineralizers

The frit and the color were ball-milled adding water (40% approx.), and the as obtained slip was dip-coated onto engobbed, red-clay, single-firing ceramic biscuits. A single firing of the enamel-ceramic biscuit set was then performed in a Nanetti furnace at 1085°C, with a 45 min fast-firing scheme. $L^*a^*b^*$ color parameters of representative samples were measured with a Perkin-Elmer spectrophotometer using a standard lighting C, following the CIE-$L^*a^*b^*$ colorimetric method recommended by the CIE (Commission Internationale de l'Eclairage) [18]. On this method, L^* is the lightness axis (black (0) → white (100)), a^* is the green (−) → red (+) axis, and b^* is the blue (−) → yellow (+) axis.

3. Results and discussion

3.1. Previous characterization of raw samples and precalcines

3.1.1. XRD and SEM/EDAX characterization

XRD of raw gels and/or coprecipitates showed the presence of ammonium sulphate and/or ammonium chloride as the only crystalline phases, confirming the amorphous state of the precursor systems (apart from the remaining oxides or mineralizers added later). Figs 1 and 2 show the XRD patterns of the binary ZFC and SFC precalcines (800°C/2 h), before the addition of the remaining precursors and mineralizers. As it can be observed in Fig. 1, the characteristic vitreous halo of amorphous silica can be seen around 15–20 °2θ, which indicates that the silica still remains amorphous after the precalcine treatment of the SFC binary coprecipitate. In addition, well-formed XRD peaks corresponding to hematite (α-Fe_2O_3) also can be seen, being evidence that a complete protection or inclusion of the iron in the amorphous silica has not been accomplished. The presence of unprotected hematite in the 800°C precalcine had not been observed in a previous study [13] where a similar coprecipitate was prepared with $FeSO_4 \cdot 7H_2O$ and LUDOX silica. The much higher specific surface of the LUDOX silica with respect to the colloidal silica (Quimidroga) here employed ($\phi_{50} = 3.2$ nm for the former and around 250 nm for the later) could be an explanation, confirming the hypothesis of Bondioli *et al.* [12] that a higher protection efficiency can be accomplished with a finer silica.

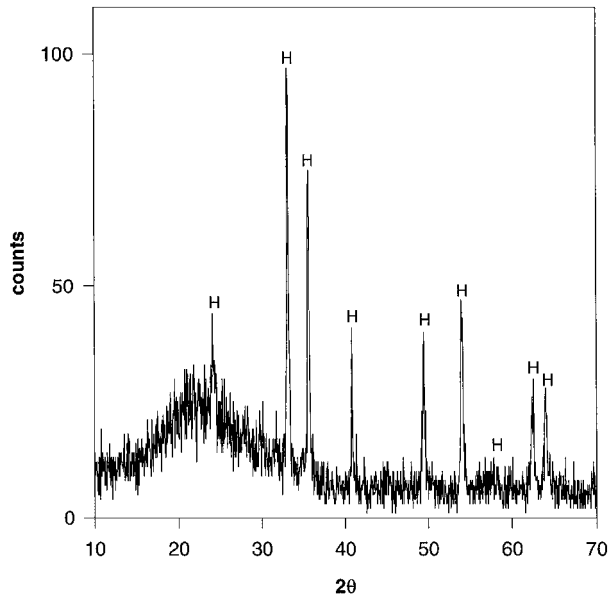

Figure 1 XRD pattern of precalcined (800°C/2 h) SFC coprecipitate. *Crystalline phases:* H (hematite, α-Fe_2O_3).

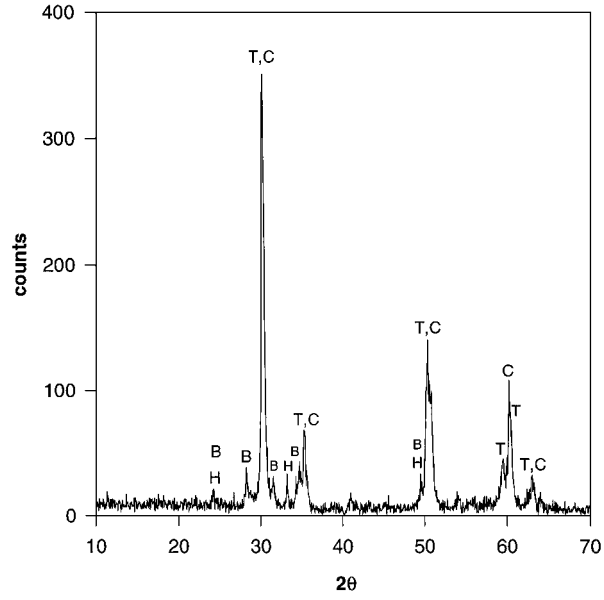

Figure 2 XRD pattern of precalcined (800°C/2 h) ZFC coprecipitate. *Crystalline phases:* T (tetragonal zirconia, ZrO_2), C (cubic zirconia, ZrO_2), B (baddeleyite or monoclinic zirconia, ZrO_2) and H (hematite, α-Fe_2O_3).

As for the ZFC precalcine (see Fig. 2), the XRD pattern confirms a significative crystallization of the tetragonal and/or cubic polymorphs of zirconia, accompanied by little XRD peaks of baddeleyite (monoclinic zirconia); in addition, weak peaks corresponding to hematite with a lower particle size (the peaks are broader) also can be observed. Thus, it seems that zirconia crystallizes first in its metastable tetragonal form when precalcining the ZFC binary colloidal gel, as it commonly happens in the calcine of Zr-containing gels or coprecipitates [19], and then the martensitic transformation from tetragonal into monoclinic zirconia starts occurring.

SEM/EDAX characterization of both SFC and ZFC precalcines was carried out to analyze the possible binary SiO_2-Fe_2O_3 and ZrO_2-Fe_2O_3 interactions occurring in the calcine, which could have an important effect on the formation of the iron zircon coral ceramic pigment. Fig. 3 shows some SEM micrographs corresponding to the SFC precalcine; the topographic images obtained with the secondary electron detector (Fig. 3a and b), let us appreciate highly amorphous silica agglomerates with sizes around 2–10 μm. At a submicronic level (Fig. 3b), these silica agglomerates are found to consist of smaller granules (around 0.25 μm), which form broad pores that coalesce in irregular channels, as previously observed by Bondioli *et al.* [12] in this system. The observations carried out with the backscattering electron emission detector (BSED) indicate, in general, an acceptable compositional homogeneity (see Fig. 3c), which means that the iron is regularly distributed or occluded within the amorphous silica agglomerates, though some heterogeneity also

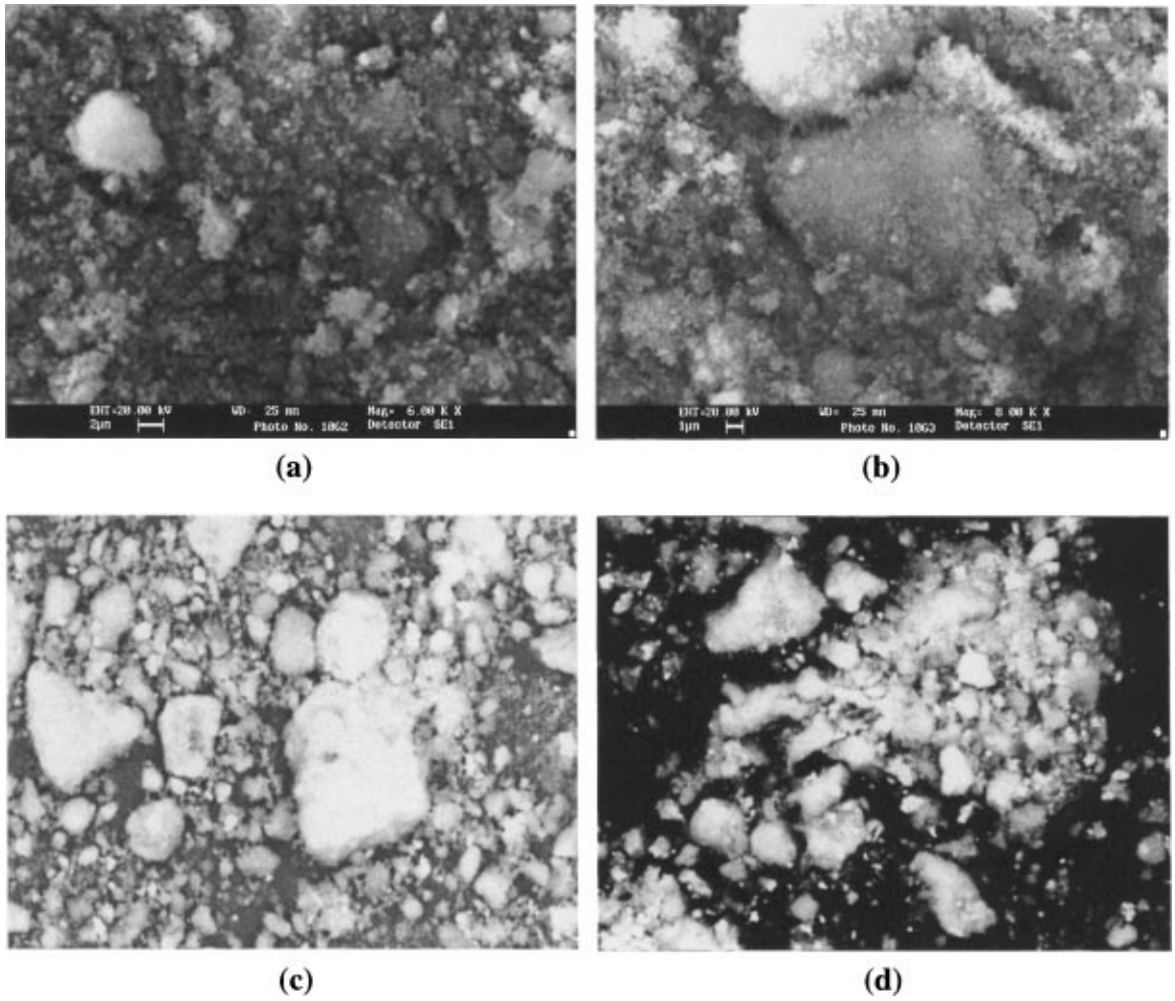

Figure 3 SEM micrographs of some details of precalcined (800°C/2 h) SFC coprecipitate: a) secondary electron detector (SED), ×6000, b) SED, ×8000, c) backscattering electron detector (BSED), ×2500 and d) BSED, ×2000.

can be observed (see the slight differences in contrast in Fig. 3d); semiquantitative analyzes obtained by EDAX at intermediate magnifications (×6000–×8000) show SiO_2/Fe_2O_3 weight ratios which in general are considerably higher than the theoretical value for the stoichiometry prepared. The presence of iron rich aggregates also was observed and confirmed by EDAX, and could be associated to hematite segregation, in agreement with the XRD characterization discussed before. Fig. 4 shows the EDAX mapping of the same field presented in Fig. 3d, along with the EDAX spectrum corresponding to a spot analysis performed on a brighter, Fe rich aggregate, confirming the existence of some heterogeneity in the Fe distribution.

Considering the precalcined ZFC binary gel, SEM observations (Fig. 5) show the presence of big monolithic zirconia agglomerates (mostly tetragonal or cubic, according to XRD characterization) with irregular forms, and with sizes ranging from 50 to 100 μm. Apart from the possible entrance of Fe^{3+} in the zirconia lattice as solid solution, which has not been analyzed in the present work, iron mainly appears to be in two different forms: i) segregated, forming Fe_2O_3 aggregates of different morphology and sizes (up to 50 μm), as the one observed in Fig. 5a; or ii) as micronic Fe_2O_3 particles (around 1–3 μm) adsorbed (or even encrusted) on the surface of the bigger zirconia monoliths, as can be seen in the BSED images shown in Fig. 5b to d. The EDAX mapping presented in Fig. 6 (accompanied by the EDAX spectrum) let us appreciate the two types of iron: along with the iron rich aggregates, some iron appears to be associated with the zirconia monoliths. The EDAX mapping of Fig. 7 (same field of Fig. 5b) obtained at a higher magnification (×3740), evidences that the micronic particles adsorbed on the surface of zirconia particles correspond to iron (α-Fe_2O_3 according to XRD characterisation). Therefore, an important ZrO_2-Fe_2O_3 surface interaction also appears to take place when firing an intimate mixture of Zr-Fe obtained by sol-gel or coprecipitation methods, as suggested in the studies of Eppler [9] and Berry *et al.* [1] with samples prepared by the traditional ceramic procedure. This surface interaction occurs to such an extent that, in any event, it must be much more relevant than the possible iron entrance in the zirconia lattice as solid solution (which can be as high as 5 wt% at 0.21 atm, according to phase equilibria studies [20]). On the other hand, SEM observations also evidence that most zirconia monoliths appear to be cracked (see Fig. 5c). The presence of these cracks extending throughout the tetragonal zirconia monoliths could be due to the mechanical stresses accumulated as a consequence of the volume gain experienced during the martensitic transformation into monoclinic zirconia, or

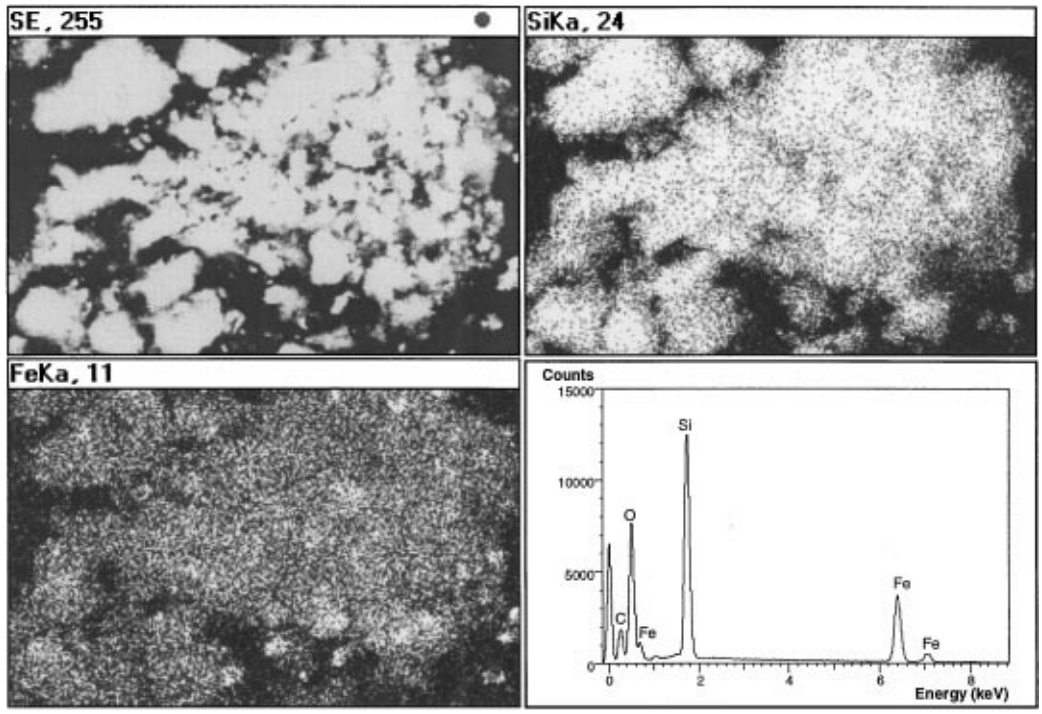

Figure 4 EDAX mapping (with BSED) and spectrum of a detail (×2400) of precalcined (800°C/2 h) SFC coprecipitate.

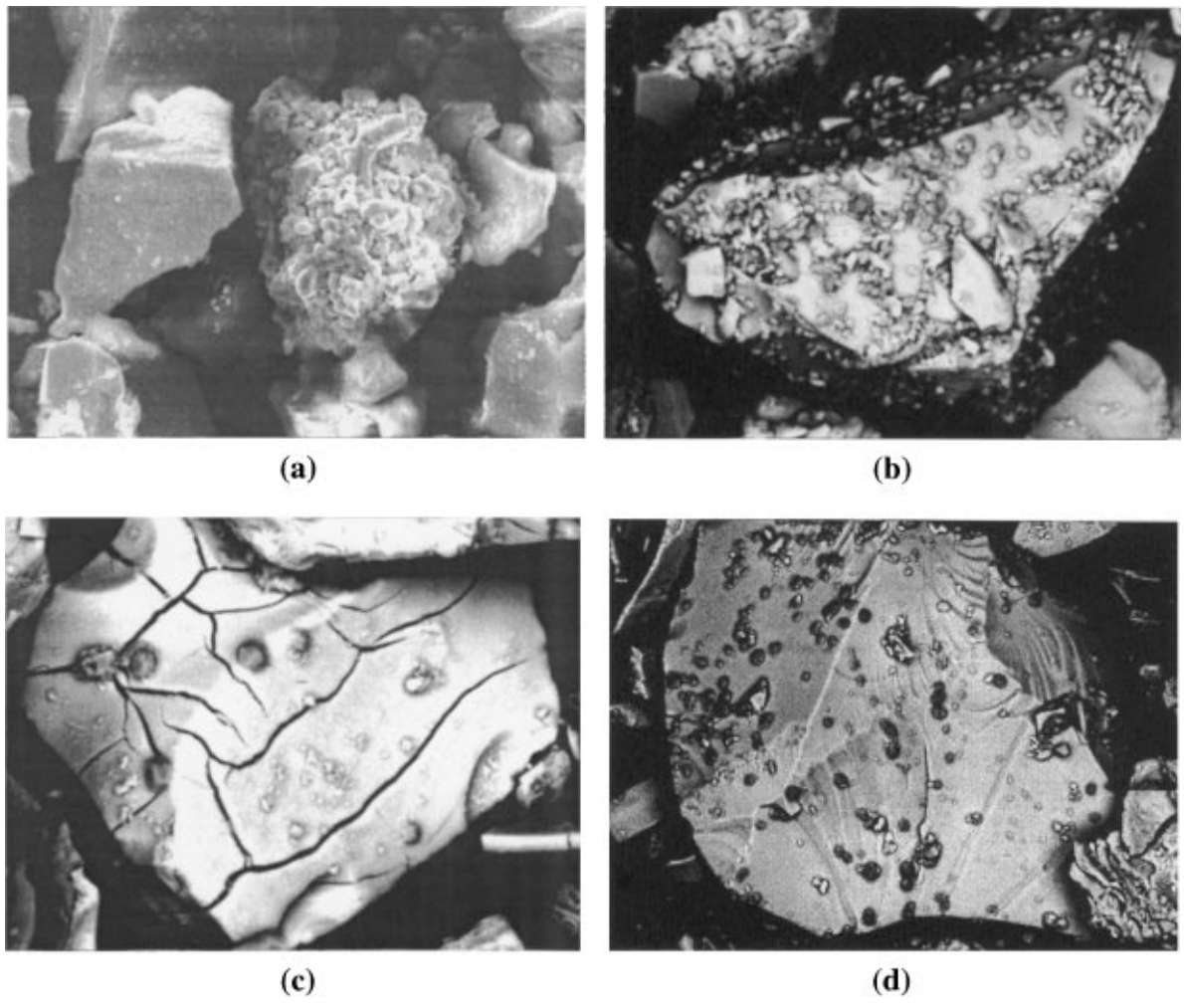

Figure 5 SEM micrographs of some details of precalcined (800°C/2 h) ZFC colloidal gel: a) secondary electron detector (SED), ×3000, b) backscattering electron detector (BSED), ×3500, c) BSED, ×4500 and d) BSED, ×2000.

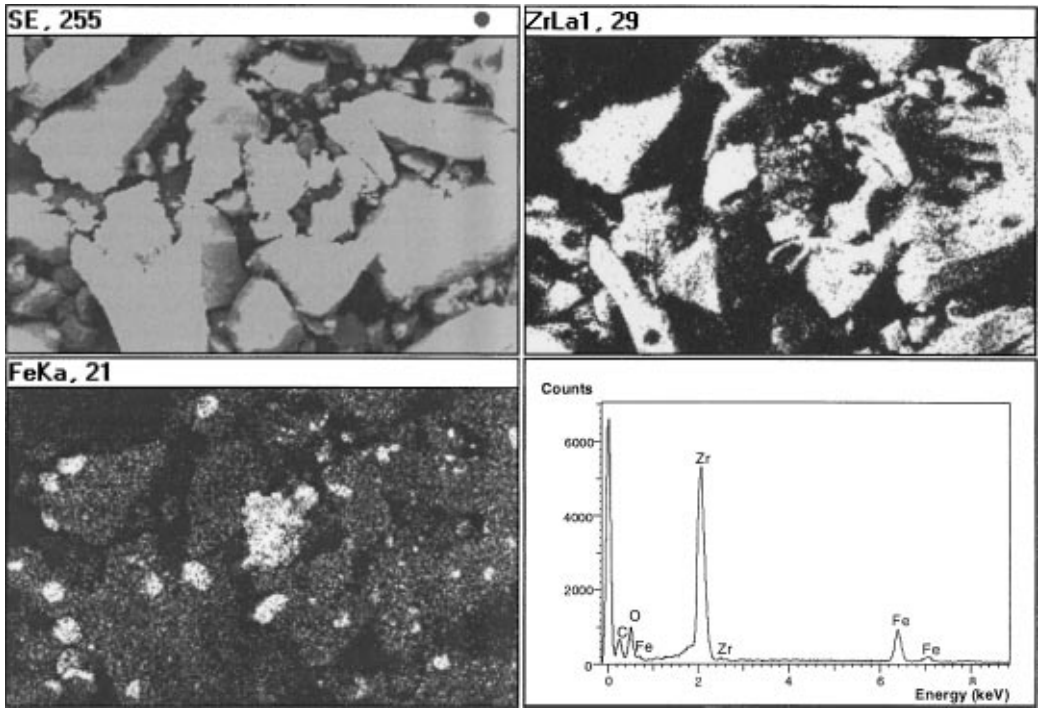

Figure 6 EDAX mapping (with SED) and spectrum of a detail (×1000) of precalcined (800°C/2 h) ZFC colloidal gel.

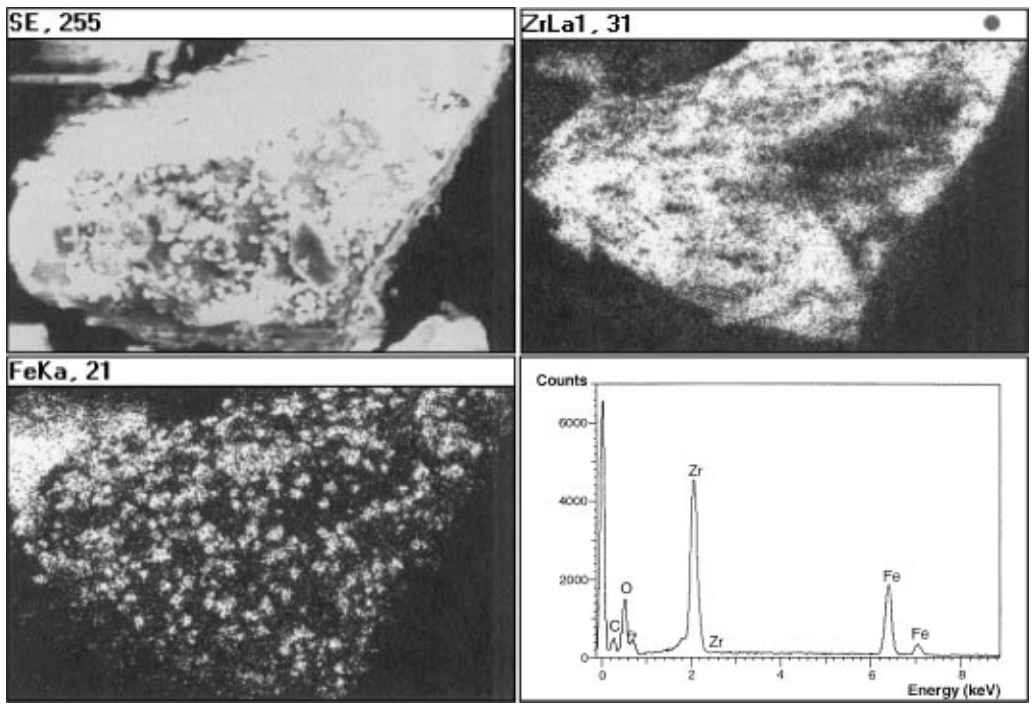

Figure 7 EDAX mapping (with SED) and spectrum of a detail (×3740) of precalcined (800°C/2 h) ZFC colloidal gel.

even due to the stresses arising from the crystalline growth of the iron particles adsorbed or encrusted on the surface.

In conclusion, the XRD and SEM/EDAX characterization performed on the SFC and ZFC precalcines has proved that important SiO_2-Fe_2O_3 and ZrO_2-Fe_2O_3 binary interactions occur when firing intimate mixtures of these components. On the one side, Fe_2O_3 readily becomes occluded in amorphous silica agglomerates, which a protection efficiency that strongly depends on the specific surface of the silica precursor employed. On the other side, along with an important iron segregation and with the possible Fe^{3+} forming a solid solution in the tetragonal zirconia lattice, micronic α-Fe_2O_3 particles become adsorbed or even encrusted on the surface of bigger tetragonal zirconia monoliths, which transform into its monoclinic form as the thermal treatment proceeds. Both processes, the iron occlusion in silica agglomerates, and the iron adsorption on the surface of zirconia monoliths, could be relevant as reaction intermediates to facilitate the hematite encapsulation in the formation of the iron zircon coral pigment, following the general coarsening-occlusion model previously proposed.

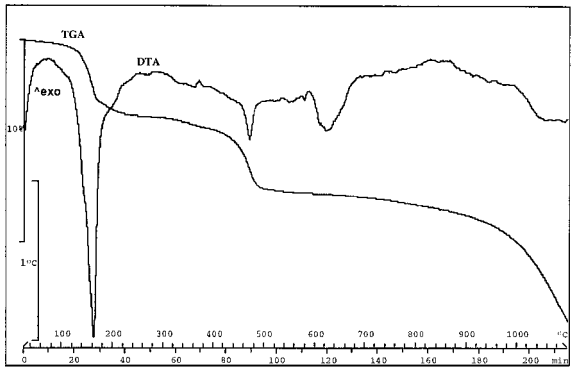

(a)

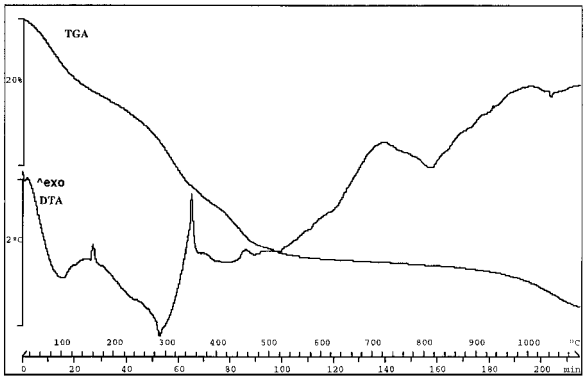

(b)

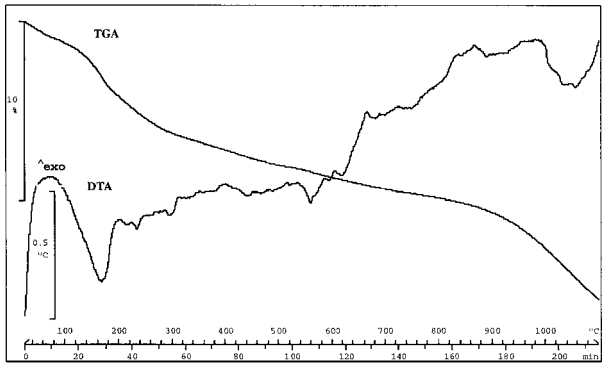

(c)

Figure 8 DTA/TGA curves corresponding to samples CER (a), ZFC1 (b) and SFC1 (c).

3.1.2. Thermal analysis (DTA/TGA)

In order to have a previous information about the behavior of the samples during the firing treatment, a thermal characterization was performed on representative raw samples. The DTA and TGA curves corresponding to CER, ZFC1 and SFC1 samples are shown in Fig. 8.

In the calcination of the reference ceramic composition (see Fig. 8a), the loss of the water molecules of the $FeSO_4.7H_2O$ employed as precursor seems to take place at 160°C (first six molecules) and at 360°C (the seventh molecule), while the sulphate decomposition occurs at 470°C. A significative endothermic band also can be observed in the DTA curve at about 620°C, which is not accompanied by any important weight loss in the TG curve. Although this band could be associated with some kind of surface interaction between iron and zirconia oxides, as suggested in the literature by Eppler [9], it seems more reasonable to associate this band around 620°C with the formation of a flux glassy phase between NaCl and NaF, in agreement with the study of Berry *et al.* [10]. On the other hand, a 4% weight loss also may be observed from 1000°C, with an endothermic effect in the DTA curve. XRD of the DTA/TGA residue showed the presence of strong intensity baddeleyite peaks, together with weak peaks of zircon, hematite and sodium sulphate. Both, the absence of unreacted quartz and the presence of a little quantity of sodium sulphate in the residue could be explained, as suggested by Berry *et al.* [9], by the existence of an interaction among the ferrous sulphate, silica and NaF, resulting in the formation of Na_2SO_4 and of the volatile SiF_4, and followed by iron oxidation to α-Fe_2O_3. Accordingly, the weight loss observed from 1000°C could be assigned to the volatilization of silicon-fluoride species and also to the decomposition of the sodium sulphate formed during the calcine. This weight loss also could be caused by the partial reduction of hematite to magnetite, though this phase was not detected by XRD in the residue.

In the case of ZFC1 sample (see Fig. 8b), broad endothermic bands are first observed at 100, 220 and 300°C, also accompanied by a huge weight loss (above 20%); the first two bands could be attributed to the loss of hydration water, while the later may be associated to the loss of sulphates and/or chlorides. In fact, ammonium sulphate and ammonium chloride (both present in the raw ZFC1 sample) decompose or sublimate at about 235°C and 340°C, respectively. The narrow exothermic peak appearing in the DTA curve around 350°C could be due to some early crystallization arising from the condensed gel network, though a clear assignment cannot easily be done. In addition, two broad exothermic bands also can be appreciated around 700 and 1000°C, which may be related to tetragonal zirconia and zircon crystallization, respectively. In this respect, XRD of the DTA/TGA residue showed the presence of strong intensity baddeleyite peaks, along with medium peaks of tetragonal zirconia and zircon, and weak hematite peaks. Therefore, ZFC1 sample seems to behave in the calcine similarly to the binary ZFC gel: tetragonal zirconia first crystallizes to later transform martensitically into monoclinic zirconia, which then reacts with silica to render zircon. Moreover, a slight weight loss also occurs from 1000°C, as with the ceramic sample, which could be due to the volatilization of silicon-fluoride species (quartz is not detected in the residue), and to a less extent to the decomposition of sodium sulphate and/or to the partial reduction of hematite to magnetite (both phases were not detected in the DTA/TGA residue). In this respect, the formation of sodium sulphate as a reaction intermediate is less probable in this sample, since SO_4^{2-} and Fe^{2+} species are chemically retained in the precursor condensed gel network together with Zr^{4+} ions (ZFC colloidal gel used as precursor), and therefore the mechanism of reaction must be different to that of the ceramic sample (ferrous sulphate molecules cannot freely interact with mineralizers).

Finally, the DTA/TGA curves corresponding to SFC1 sample may be seen (Fig. 8c) to present some differences: first, the loss of hydration water is observed to

occur around 150°C (strong endothermic band with an associated 5% weight loss), and then a slight and continuous weight loss occurs from 280 up to 940°C. The DTA curves present weaker endothermic signals at 240, 310, 430, 560°C (this one slightly more intense) and 620°C, difficult to assign (the weak band at 620°C could be due to the formation of a glassy phase between NaF and NaCl, as in CER sample), and then a broad exothermic band extends from 700 up to 1000°C, which could be attributed to hematite and silica crystallization. Similarly to previous samples, a weight loss is observed from 1000°C, with an associated endothermic peak in the DTA curve. This weight loss, as explained before, could probably arise from the volatilization of silicon-fluoride species, and/or from the decomposition of the sodium sulphate (strong intensity peaks of baddeleyite were detected by XRD in the residue, together with very weak peaks of hematite, zircon and sodium sulphate).

3.2. Characterization of the fired and enameled pigments

Table II summarizes the XRD crystalline phases present in the fired pigments (950°C/2 h 30 min), the Fe^{3+} and SO_4^{2-} concentrations leached in washing waters, as well as the $L^*a^*b^*$ colorimetric parameters measured with the enameled samples (with 5 wt-% color).

Sample SFC1 (prepared with a Si-Fe raw coprecipitate as Si-Fe precursor) stands out for its reactivity (the zircon yield accomplished is even higher than that of the reference ceramic composition) and also for its pink coral hue, similar to that of the ceramic sample. In fact, SFC1 and CER samples produce the best coral colors, with a much higher value of the parameter representative of the red color, (a^* above 29, which is similar to the value presented by commercial coral pigments), and with a lower L^* value (darker and intenser colors). Accordingly, the protection or occlusion of α-Fe_2O_3 in amorphous silica agglomerates of high specific surface, appears to be an effective reaction intermediate for the pigment formation.

On the other hand, the employment in sample ZFC1 of a raw, intimate mixture of Zr and Fe precursors (ZFC) prepared by the aqueous sol-gel processing, does not produce a positive effect on the synthesis of the iron zircon coral pigment: in spite of the acceptable zircon yield obtained, the measured coral or red color results to be the poorest ($a^* = 7.5$). This result is in contrast with the improved iron zircon pink pigment that can be obtained, according to Eppler [9], from intimate ZrO_2-Fe_2O_3 mixtures prepared by the traditional ceramic procedure. Even the employment as precursor of a complete colloidal gel including all the precursors and mineralizers (sample CC) leads to a more intense pink coral pigment ($a^* = 17.8$) than ZFC1 (though still less intense than CER and SFC1 samples).

In addition, the effect of precalcining at 800°C the SFC coprecipitate or the ZFC gel before the addition of the remaining precursors and mineralizers (samples

TABLE II Characterisation of the fired pigments

Sample	XRD crystalline phases	$[SO_4^{2-}]$ (ppm)	$[Fe^{3+}]$ (ppm)	L^*	a^*	b^*
CER	Z(s), B(vw), H(vw)	552	3.1	55.7	29.5	24.2
CC	Z(m-s), B(vw), H(vw-w)	525	0.8	70.3	17.8	26.6
SFC1	Z(vs), B(vw), H(vw)	336	0.8	59.6	29.3	25.8
SFC2	Z(m), B(w-m), H(vw)	25	15.1	70.3	22.2	24.6
ZFC1	Z(m-s), B(vw), H(vw)	443	0.6	81.0	7.5	26.7
ZFC2	Z(m-s), B(w), H(vw)	28	8.0	73.0	13.5	22.3

Crystalline phases: Z (zircon, $ZrSiO_4$), B (baddeleyite, ZrO_2), and H (hematite, α-Fe_2O_3); *XRD peaks intensity*: vs (very strong), s (strong), m (medium), w (weak), ad vw (very weak).

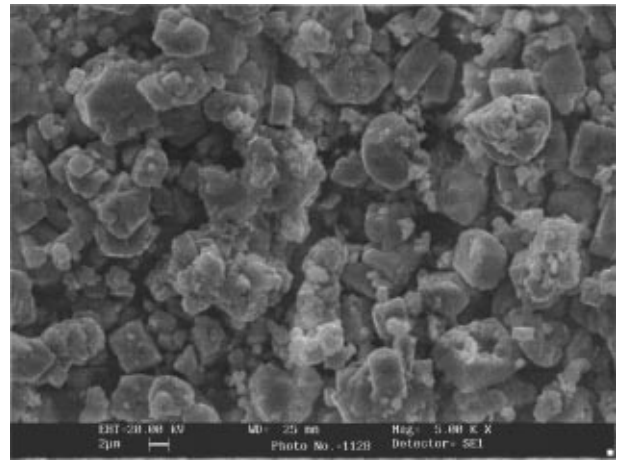

(**a**)

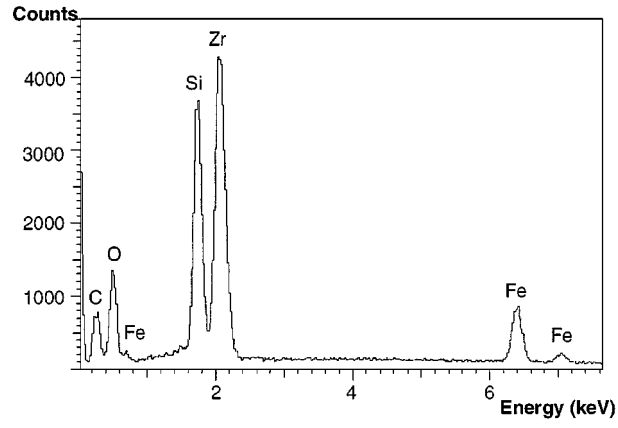

(**b**)

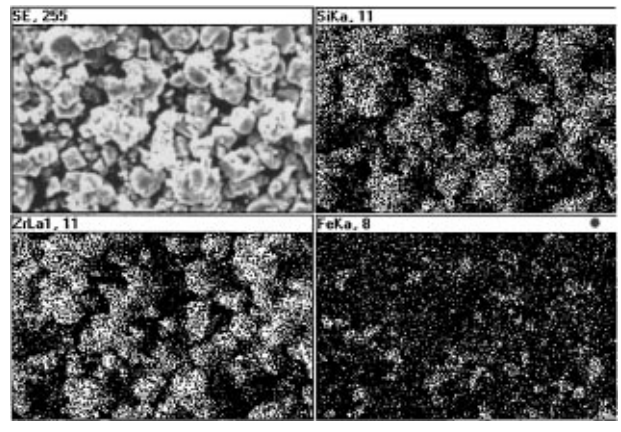

(**c**)

Figure 9 SEM micrograph -SED ×5000- (a), EDAX spectrum (b), and EDAX mapping (c) of a detail of CER fired pigment (950°C/2 h).

SFC2 and ZFC2), is found to be different in each case. As for the SFC2 sample, the precalcine proves to have a negative effect on both, the reactivity (a much lower zircon yield is obtained) and the coloring performance (lower a^*). In this respect, the loss of silica as volatile silicon-fluorine species during the final calcine could have been triggered by this precalcine (Berry *et al.* [9] detect the volatilization of SiF_3 species between 600 and 800°C, probably as a breakdown product of SiF_4), which would account for the lower zircon yield accomplished, for the absence of unreacted quartz, and also for the presence of an important quantity of unreacted zirconia in the XRD pattern of SFC2 sample. On the contrary, the precalcine of the ZFC gel results to have a positive effect, considering the improved red color of sample ZFC2 with respect to ZFC1 ($a^* = 13.5$ against 7.5). This fact, together with the less intense red colors obtained with samples CC, ZFC1 and ZFC2 could be explained considering that the necessary transformation of tetragonal zirconia into its monoclinic form prior to the zircon formation would interfere in the effectiveness of the hematite occlusion in these samples. In fact, when this transformation is accelerated, for instance by precalcining the ZrO_2-Fe_2O_3 mixture in ZFC2 sample, therefore an improvement in the red color of the pigment is obtained.

On the other hand, a direct relationship between the coloring yield and the iron extracted in washig waters cannot be made, since the Fe^{3+} concentration in washing waters is not always observed to diminish, the intenser the red color (higher a^* value).

Finally, a microstructure characterization of the optimal CER and SFC1 fired pigments was carried out. Figs 9 and 10 show two SEM micrographs of fired CER and SFC1 pigments, respectively, along with the EDAX spectrum and mapping of the same fields. The microstructure of these two samples is found to be very similar: in both cases, a bimodal size distribution of zircon particles can be observed, with 4–6 μm sized particles predominating with respect to accompanying finer particles (around 1 μm). EDAX analysis indicates a higher iron content in SFC1 than in the ceramic sample, which may be associated with a higher hematite segregation in the former as can be seen in the corresponding EDAX mappings.

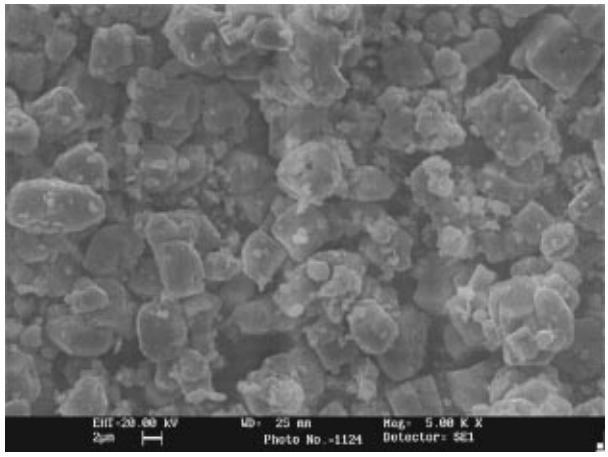

(**a**)

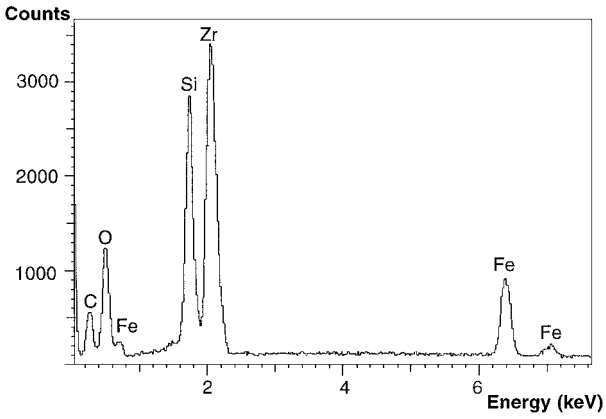

(**b**)

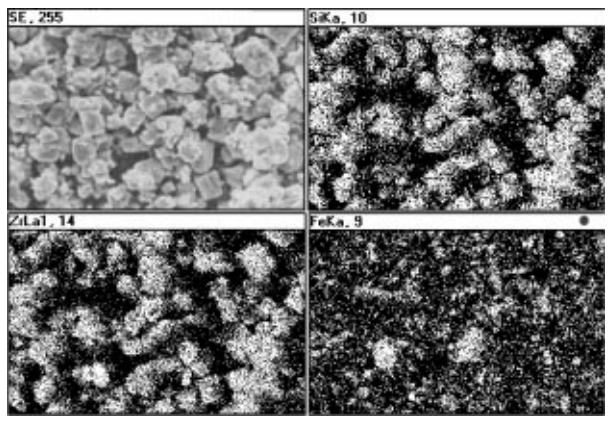

(**c**)

Figure 10 SEM micrograph -SED ×5000- (a), EDAX spectrum (b), and EDAX mapping (c) of a detail of SFC1 fired pigment (950°C/2 h).

4. Conclusions

i) Relevant binary interactions have been found to occur in the calcine of Si-Fe and Zr-Fe coprecipitates (or colloidal gels) employed as precursors in the synthesis of the iron zircon coral ceramic pigment: α-Fe_2O_3 readily becomes occluded in amorphous silica agglomerates of high specific surface, while micronic α-Fe_2O_3 particles to a great extent become adsorbed or even encrusted on the surface of tetragonal zirconia monoliths.

ii) The use of a binary coprecipitate as precursor prepared with colloidal silica and ferrous sulphate leads to a more intense coral hue ($L^* = 59.6$, $a^* = 29.3$ and $b^* = 25.8$ at 950°C), than the employment of binary ZrO_2-Fe_2O_3 (raw or precalcined) or complete ZrO_2-SiO_2-Fe_2O_3 aqueous gels; in the later, the α-Fe_2O_3 segregation and the necessary transformation of tetragonal zirconia into its monoclinic form prior to zircon formation, seem to lower the efficiency of hematite encapsulation in the zircon matrix, following the coarsening-occlusion process involved in the pigment formation.

iii) the precalcine of the binary SFC coprecipitate containing silicon and iron precursors has a negative effect on the synthesis of the coral pigment, as a result of the stoichiometry loss caused by the formation of volatile silicon-fluoride species. On the contrary, the precalcine of the ZFC colloidal gel containing zirconium and iron precursors has a positive effect, since it produces an advance in the necessary transformation from tetragonal to monoclinic zirconia.

Acknowledgements

Mario Llusar is grateful to the *Conselleria de Cultura, Educació i Ciència de la Generalitat Valenciana* for his research grant.

References

1. F. J. BERRY, D. EADON, J. HOLLOWAY and L. E. SMART, *J. Mater. Chem.* **6** (1996) 221.
2. I. GAIR, R. H. JONES, A. C. AIREY, G. SANKAR and D. GLEESON, Communication presented in the *VI World Congress on the Quality of Wall and Floor Ceramic Tiles* (*QUALICER*), Castellón (Spain), March of 2000.
3. A. C. AIREY and W. ROBERTS, *Ceram. Eng. Sci. Proc.* **8** (1987) 1168.
4. J. LAHUERTA, PhD thesis, Universitat de València (Spain), June 1993.
5. M. LLUSAR, PhD thesis, Universitat Jaume I de Castelló (Spain), September 1998.
6. M. LLUSAR, J. A. BADENES, J. CALBO, M. A. TENA and G. MONRÓS, *Brit. Ceram. Trans.* **99** (2000) 14.
7. R. A. EPPLER, *J. of Amer. Ceram. Soc.* **62** (1979) 247.
8. *Idem., ibid.* **53** (1979) 457.
9. C. LI and R. A. EPPLER, *Ceram. Eng. Sci. Proc.* **13** (1992) 109.
10. F. J. BERRY, D. EADON, J. HOLLOWAY and L. E. SMART, *J. Mater. Sci.* **34** (1999) 3631.
11. P. TARTAJ, T. GONZALEZ-CARREÑO, C. J. SERNA and M. OCAÑA, *J. of Solid State Chem.* **128** (1997) 102.
12. F. BONDIOLI, A. M. FERRARI, C. LEONELLI and T. MANFREDINI, *Mat. Res. Bull.* **33** (1998) 723.
13. J. B. VICENT, M. LLUSAR, J. A. BADENES, M. A. TENA and G. MONRÓS, *Bol. Soc. Esp. Ceram. Vidr.* **39** (2000) 83.
14. A. C. PIERRE, *Ceram. Bull.* **70** (1991) 1281.
15. G. MONRÓS, M. A. TENA, P. ESCRIBANO, V. CANTAVELLA and J. CARDA, *J. Sol-Gel Sci. Technol.* **2** (1994) 377.
16. M. LLUSAR, G. MONRÓS, M. A. TENA, J. B. VICENT and J. A. BADENES, *Brit. Ceram. Trans.* **98** (1999) 1.
17. W. HELLER, in "Polymer Colloids 2," edited by M. Fitch (Plenum, New York, 1980).
18. CIE, Reccommendations on Uniform Color Spaces, Color Difference Equations, Psychometrics Color Terms. Suplement No 2 of CIE Publ. No 15 (E1-1.31) 1971, Bureau Central de la CIE, Paris, 1978.
19. G. MONRÓS, J. CARDA, P. ESCRIBANO and J. ALARCÓN, *J. Mat. Sci. Lett.* **9** (1990) 184.
20. T. S. JONES, S. KIMURA and A. MUAN, *J. Am. Ceram. Soc.* **50** (1967) 137.

Received 26 August 1999
and accepted 30 May 2000